

Quantifying Data Augmentation for LiDAR based 3D Object Detection

Martin Hahner¹, Dengxin Dai¹, Alexander Liniger¹, and Luc Van Gool^{1,2}

Abstract—In this work, we shed light on different data augmentation techniques commonly used in Light Detection and Ranging (LiDAR) based 3D Object Detection. We, therefore, utilize a state of the art *voxel* based 3D Object Detection pipeline called *PointPillars* [1] and carry out our experiments on the well established KITTI [2] dataset. We investigate a variety of *global* and *local* augmentation techniques, where *global* augmentation techniques are applied to the entire point cloud of a scene and *local* augmentation techniques are only applied to points belonging to individual objects in the scene. Our findings show that both types of data augmentation can lead to performance increases, but it also turns out, that some augmentation techniques, such as individual object translation, for example, can be counterproductive and can hurt overall performance. We show that when we apply our findings to the data augmentation policy of *PointPillars* [1] we can easily increase its performance by up to 2%. In order to provide reproducibility, our code will be publicly available at www.trace.ethz.ch/3D_Object_Detection.

I. INTRODUCTION

The last years have seen tremendous progress in 3D Object Detection for autonomous driving and the task really only emerged in 2017, when the KITTI [2] dataset, originally introduced in 2012, was extended by novel benchmarks for 3D Object Detection including 3D and bird’s eye view (BEV) evaluation. Since then, many more publicly available LiDAR datasets with 3D bounding box annotations have followed. nuScenes [3], Lyft Level 5 AV Dataset [4], Waymo Open Dataset [5], Argoverse [6], Apollo 3D [7] and Honda 3D [8], just to name some of them. With LiDAR sensors getting cheaper [9] and thereby becoming a viable option for autonomous driving, these LiDAR datasets are fundamental to improve the current state of the art in LiDAR based 3D Object Detection.

Further, the motivation behind the task of 3D Object Detection is that autonomous driving cars need to find a trajectory in the real world (a 3D space) and not only in a 2D image space. Hence, 2D Object Detection for example is insufficient since 2D Object Detection only delivers a location and dimensions in the image plane. Even when 2D Object Detection results are merged with Depth Estimation for example through a stereo camera setup, the performance is not as high as directly reasoning in a 3D LiDAR point cloud. In fact, the best camera based approach we know of, Pseudo-LiDAR [10], utilizes a 3D Object Detection pipeline.

What they propose is to convert image-based depth maps into pseudo-LiDAR representations (essentially fake point clouds) and show that this is a much better representation to detect objects in 3D compared to utilizing purely image processing pipelines. Image based 3D Object Detection might just be too ill-posed, which makes us believe that in order to reach the desired level of safety for autonomous driving cars, in the end we probably need to have a sensor on-board that is able to deliver raw 3D depth information.

To specify the task at hand, what we are looking for in 3D Object Detection for autonomous driving are specifically seven degrees of freedom as opposed to only four in 2D Object Detection. In the task of 3D Object Detection we want to predict the center position of an object x_c, y_c, z_c , its dimensions w, l, h and the *yaw* angle θ (rotation around the upright axis). And since data augmentation for 3D Object Detection has been found crucial by many works [11], [12], [13], especially on the KITTI [2] dataset with its limited amount of training samples, we wanted to investigate data augmentation for LiDAR based 3D Object Detection in greater detail. Given our findings (presented in Section IV), we believe that such an extensive augmentation study has been long overdue.

The contributions in our paper are three-fold, first and foremost, we present an in-depth study of augmentation methods for LiDAR based 3D Object Detection. This study allows practitioners to short cut time consuming experiments and get good results quicker. Second, we show some non-intuitive results, for example, translation of objects can reduce performance, or that excluding *hard* cases from training can increase the performance for these *hard* cases during evaluation. These findings pose new research questions and suggest some insight how 3D Object Detection networks might work internally. Finally, based on our study of augmentation methods, we propose a new augmentation policy that is able to increase the performance of *PointPillars* [1] by up to 2%.

II. RELATED WORK

Up until now, most LiDAR based 3D Object Detection methods can be categorized into one out of three categories:

- *Voxel based 3D Object Detection* (section II-A),
- *Point based 3D Object Detection* (section II-B) and
- *Voxel & Point based 3D Object Detection* (section II-C).

In the following subsections, we will give a detailed literature review about these three categories.

¹Martin Hahner, Dengxin Dai, Alexander Liniger and Luc Van Gool are all with the Toyota TRACE-Zurich team at the Computer Vision Lab, ETH Zurich, 8092 Zurich, Switzerland. firstname.lastname@vision.ee.ethz.ch

²Luc Van Gool is also with the Toyota TRACE-Leuven team at the Dept. of Electrical Engineering ESAT, KU Leuven, 3001 Leuven, Belgium. luc.vangool@kuleuven.be

A. Voxel based 3D Object Detection

The earliest works in this line of work include MV3D [14], PIXOR [11] and AVOD [15]. They all divide the 3D space into a voxel grid. Then they use hand-crafted features (e.g. point count per voxel) and hand-crafted neighborhood features (e.g. maximum point count per pillar). In the end, they have a 3D Tensor of neighborhood features (x, y, c) and apply regular 2D convolutions on them. The drawback of these methods mostly lies in the hand-crafted feature design.

VoxelNet [12] is one of the seminal works in the area of 3D Object Detection, as a first, this work presents a 3D Object Detection pipeline in an end-to-end fashion without any hand-crafted features. They apply a PointNet-like [16] architecture to every individual voxel leading to a 4D Tensor (x, y, z, c) . Then they perform 3D convolutions to consolidate the z -dimension and get a 3D Tensor (x, y, c') . Only then they utilize a region proposal network (RPN) based on 2D convolutions.

Another significant contribution to the area of LiDAR based 3D Object Detection is SECOND [13], they were able speed up the bottleneck of earlier works, the 3D convolutions, by implementing a sparse 3D convolution layer.

Based on their code-base, PointPillars [1] gets entirely rid of the z -dimension by only dividing the 3D space into pillars instead of voxels. This change by itself gives a 10-100x speed-up compared to VoxelNet [12]. Additionally, to further speed up the novel encoder, they process each pillar only using a single 1x1 convolution + max-pooling layer instead of a more complex PointNet-like [16] architecture. In the end, their final encoder only needs 1.3ms (instead of 190ms in VoxelNet [12]).

B. Point based 3D Object Detection

First, we would like to mention PointNet [16]. PointNet laid the foundations for many applications, not just for 3D Object Detection. Their work can also be applied to point cloud Classification, Part Segmentation and Semantic Segmentation. The main reason their work is so applicable to multiple domains is because its architecture is relatively lightweight, yet highly efficient and effective, it can process up to one million points per second.

VoteNet [17] is a more recent work, that has not proven itself yet on an automotive dataset, but showed promising results on two indoor scene understanding datasets, ScanNet [18] and SUN RGB-D [19]. VoteNet is an end-to-end 3D Object Detection network based on a synergy of deep point set networks and Hough Voting which does not rely on any kind of anchors.

PointRCNN [20] is another recent work, which also does not need to utilize any anchors. It is a two-stage architecture, where the first stage generates 3D bounding box proposals from a raw point cloud in a bottom-up manner and the second stage refines the 3D bounding box proposals in a canonical representation.

C. Voxel & Point based 3D Object Detection

Both, *voxel* and *point* based 3D Object Detection methods have their strengths and weaknesses. Therefore it only comes naturally that there are methods trying to combine the best of both worlds.

Fast Point R-CNN [21] is such a method. It is a two-stage framework, where in the first stage they voxelize the point cloud and feed it to a VoxelRPN to produce a small number of initial predictions. Then, in the second stage, they fuse the features of the box with features from individual points lying inside those proposals and further refine their initial predictions from the first stage.

Point-Voxel CNN [22] is a very recent method that utilizes (coarse) voxels and directly processes the points of the point cloud. Their architecture has two branches, a *low-resolution* voxel based and a *high-resolution* point based branch. The voxel based branch extracts *coarse-grained* neighborhood information, which is supplementary to the *fine-grained* individual point features extracted from the point based branch.

III. METHOD

In this section, we present all augmentation techniques investigated in this paper. They can be categorized into four categories:

- *global* augmentations (section III-A),
- *local* augmentations (section III-B),
- *filter* augmentations (section III-C) and
- *oversampling* (section III-D).

A. Global Augmentation

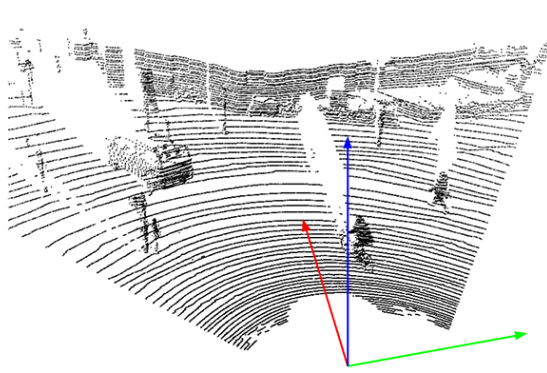
Global augmentations are applied to the all points in the point cloud $P = \{p_0, \dots, p_n\}$ and all annotations $A = \{a_0, \dots, a_m\}$ simultaneously. A visualization of all *global* augmentation techniques investigated in this paper are shown in Fig. 1 applied to an example scene (Fig. 1a).

1) Global Translation:

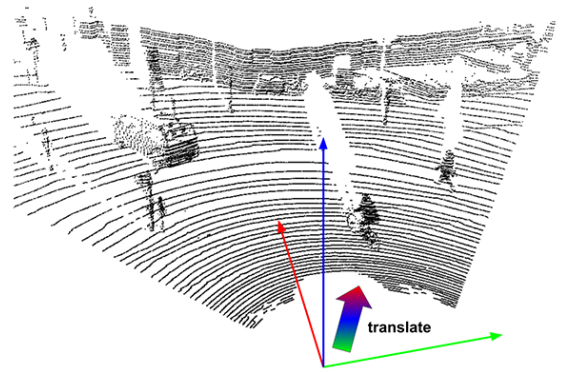
Global translation (Fig. 1b) means that we are translating every point $p(x, y, z) \in P$ such that an augmented point p^* has the form $p(x + \Delta x, y + \Delta y, z + \Delta z)$. Simultaneously, we shift every annotation $a(x_c, y_c, z_c, w, l, h, \theta) \in A$ such that an augmented annotation a^* has the form $a(x_c + \Delta x, y_c + \Delta y, z_c + \Delta z, w, l, h, \theta)$. Therefore we independently sample $\Delta x, \Delta y$ and Δz from a normal distribution $N(0, \sigma^2)$ where σ can take the following values $\sigma^2 \in \{0.1, 0.2, 0.4\}m$.

2) Global Rotation:

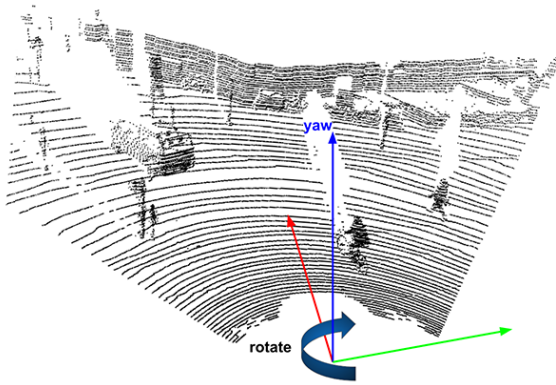
Global rotation (Fig. 1c) means that we are rotating every point $p(x, y, z) \in P$ around the upright *yaw* axis by an angle α drawn from a uniform distribution $U(-\beta, +\beta)$ where $\beta \in \{\pi/8, \pi/4, \pi/2\}$. Simultaneously, we rotate every annotation $a(x_c, y_c, z_c, w, l, h, \theta) \in A$ such that the augmented annotation a^* has the form $a(x_c, y_c, z_c, w, l, h, (\theta + \alpha) \bmod 2\pi)$.



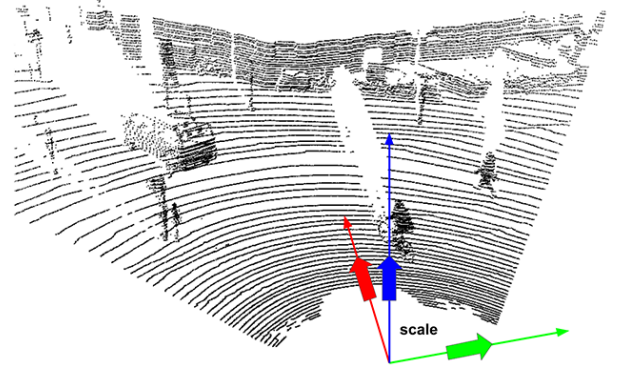
(a) Original scene.



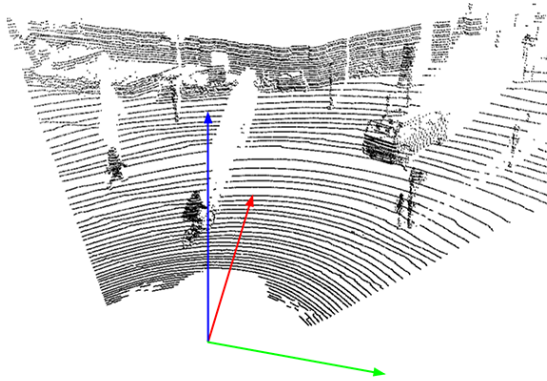
(b) *Global Translation* (section III-A.1).



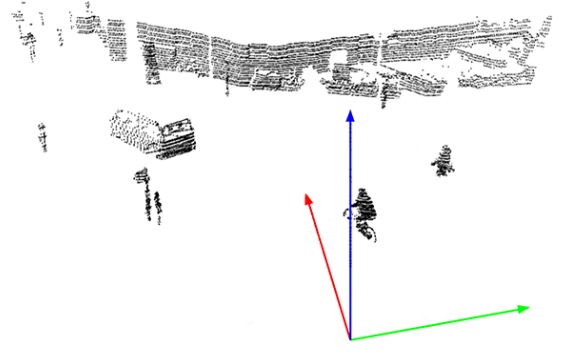
(c) *Global Rotation* (section III-A.2).



(d) *Global Scaling* (section III-A.3).

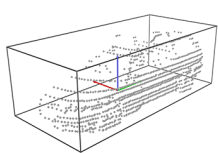


(e) *Random Flip* (section III-A.4).

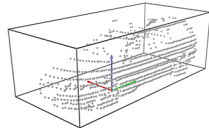


(f) *Ground Removal* (section III-A.5).

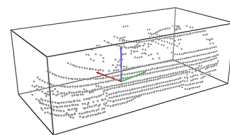
Fig. 1. Visualization of all *global* augmentation techniques investigated in this paper.



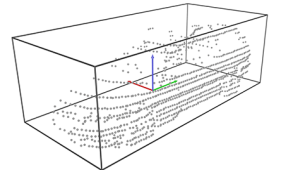
(a) Original annotation.



(b) *Local Translation* (section III-B.1).



(c) *Local Rotation* (section III-B.2).



(d) *Local Scaling* (section III-B.3).

Fig. 2. Visualization of all *local* augmentation techniques investigated in this paper.

3) Global Scaling:

Global scaling (Fig. 1d) means that we are scaling every point $p(x,y,z) \in P$ in every direction by a scalar s drawn from a uniform distribution $U(1-t, 1+t)$ where $t \in \{0.05, 0.1, 0.25\}$ such that an augmented point p^* has the form $p(s \cdot x, s \cdot y, s \cdot z)$. Simultaneously, we scale every annotation $a(x_c, y_c, z_c, w, l, h, \theta) \in A$ such that an augmented annotation a^* has the form $a(s \cdot x_c, s \cdot y_c, s \cdot z_c, s \cdot w, s \cdot l, s \cdot h, \theta)$.

4) Random Flip:

Random flip (Fig. 1e) means that we flip every point $p(x,y,z) \in P$ by a 50% chance on the forward facing x -axis. So if we flip the whole point cloud, an augmented point p^* has the form $p(x, -y, z)$. Simultaneously, if we flip every point $p(x,y,z) \in P$, we also flip every annotation $a(x_c, y_c, z_c, w, l, h, \theta) \in A$ such that an augmented annotation a^* has the form $a(x_c, -y_c, z_c, w, l, h, (\theta + \pi) \bmod 2\pi)$. We do not flip on the sideways facing y -axis because KITTI [2] only provides 3D bounding box annotations in the camera field of view. So it does not make sense to flip on the y -axis when on the other side, there are no targets to train for.

5) Ground Removal:

Ground removal (Fig. 1f) means that we remove every point $p(x,y,z) \in P$ where z is smaller than a threshold $\epsilon \in \{1\text{st}, 5\text{th}, 10\text{th}, 15\text{th}\}$ percentile of all z -values in the point cloud P . The idea behind this is to get rid of “background” points, because a LiDAR point cloud is typically very unbalanced in terms of “foreground” vs. “background”. In the KITTI [2] training set for example, there are on average 19,047 points per scene in the camera field of view and only 1,382 points ($\approx 7.25\%$) thereof lie inside 3D bounding box annotations (“foreground”). For the KITTI [2] validation set, this statistic does not look much different, there are on average 18,888 points per scene in the camera field of view and 1,641 points ($\approx 8.69\%$) thereof lie inside 3D bounding box annotations. This augmentation also has the uniqueness, that it is the only augmentation we investigate, that is applied during training and testing. This is to not mess up the distribution of “foreground” vs. “background” during the different stages. All other augmentations are only applied during the training stage.

B. Local Augmentation

Similar to the *global* augmentation techniques presented in the previous section, *local* augmentations presented in this section also involve translation, rotation and scaling. The only difference is, that here we do not apply those transformations to every point $p(x,y,z) \in P$, but only to individual annotations and the points that reside inside those annotations. Thereby we augment every annotation independently from every other, meaning that for every annotation we draw a different random value. A visualization of all *local* augmentation techniques investigated in this paper are shown in Fig. 2 with an example annotation (Fig. 2a).

1) Local Translation:

Local translation (Fig. 2b) means that we are translating every point $p(x,y,z) \in a$ such that an augmented point p^* has the form $p(x + \Delta x, y + \Delta y, z + \Delta z)$. Simultaneously, we shift the annotation $a(x_c, y_c, z_c, w, l, h, \theta)$ such that an augmented annotation a^* has the form $a(x_c + \Delta x, y_c + \Delta y, z_c + \Delta z, w, l, h, \theta)$. Again, we independently sample $\Delta x, \Delta y$ and Δz from a normal distribution $N(0, \sigma^2)$, with $\sigma^2 \in \{0.05, 0.25, 0.5, 1\}\text{m}$.

2) Local Rotation:

Local rotation (Fig. 2c) means that we are rotating every point $p(x,y,z) \in a$ around the upright *yaw* axis by an angle α drawn from a uniform distribution $U(-\beta, +\beta)$ where $\beta \in \{\pi/20, \pi/10, \pi/4\}$. Simultaneously, we rotate the annotation $a(x_c, y_c, z_c, w, l, h, \theta)$ such that the augmented annotation a^* has the form $a(x_c, y_c, z_c, w, l, h, (\theta + \alpha) \bmod 2\pi)$.

3) Local Scaling:

Local scaling (Fig. 2d) means that we are scaling every point $p(x,y,z) \in P$ in every direction by a scalar s drawn from a uniform distribution $U(1-t, 1+t)$ where $t \in \{0.05, 0.1, 0.25\}$ such that an augmented point p^* has the form $p(s \cdot x, s \cdot y, s \cdot z)$. Simultaneously, we scale every annotation $a(x_c, y_c, z_c, w, l, h, \theta) \in A$ such that an augmented annotation a^* has the form $a(s \cdot x_c, s \cdot y_c, s \cdot z_c, s \cdot w, s \cdot l, s \cdot h, \theta)$.

C. Filter Augmentations

Filter augmentations are pretty straightforward. One way to filter annotations is to filter them based on their difficulty. In KITTI [2] there are three predefined difficulties: *easy*, *moderate* and *hard*, where some annotations are also labeled as *unknown*.

Another simple filter operation is to exclude annotations from training when they contain less than a certain amount of LiDAR points inside of them. In our experiments, we investigated a minimum threshold of 1, 5 and 10 points.

D. Oversampling

Oversampling means that we are trying to sample additional cars from other scenes into the current scene. In order to do this, one has to iterate over all annotations once and construct a database of annotations and their corresponding points. This “trick” also aims at balancing the “foreground” vs. “background” imbalance described earlier. During training, one only has to check whether the additionally sampled annotations from the database do not collide with any of the ones originally present in the current scene. In our experiments we tried to oversample to 5, 10, 15, 20 and 25 annotations. If there is a collision, those annotations are discarded and only the ones that do not collide are kept. This means for example in the setting where we try to sample up to 15 cars, at most 15 annotations are additionally sampled.

IV. EXPERIMENTS

In this section, we present the findings of our extensive augmentation study summarized in Table I.

policy #	Global Translation	Global Rotation	Global Scaling	Random Flip	Ground Removal	Local Translation	Local Rotation	Local Scaling	filter unknown	filter hard	filter moderate	filter by points	Oversampling	Car 3D ap ₄₀		
														easy	moderate	hard
0	X	X	X	X	X	X	X	X	X	X	X	X	X	71.98	59.29	55.94
1	0.1m	X	X	X	X	X	X	X	X	X	X	X	X	+6.31	+5.55	+3.93
2	0.2m	X	X	X	X	X	X	X	X	X	X	X	X	+7.21	+6.64	+5.62
3	0.4m	X	X	X	X	X	X	X	X	X	X	X	X	+4.54	+5.18	+4.47
4	X	$\pi/8$	X	X	X	X	X	X	X	X	X	X	X	+7.97	+9.10	+7.90
5	X	$\pi/4$	X	X	X	X	X	X	X	X	X	X	X	+10.34	+9.89	+8.75
6	X	$\pi/2$	X	X	X	X	X	X	X	X	X	X	X	+11.51	+10.73	+10.90
7	X	X	[0.95, 1.05]	X	X	X	X	X	X	X	X	X	X	+7.24	+6.96	+5.43
8	X	X	[0.90, 1.10]	X	X	X	X	X	X	X	X	X	X	+6.43	+5.72	+4.87
9	X	X	[0.75, 1.25]	X	X	X	X	X	X	X	X	X	X	+8.10	+5.43	+3.19
10	X	X	X	✓	X	X	X	X	X	X	X	X	X	+7.02	+6.93	+7.58
11	X	X	X	X	1%	X	X	X	X	X	X	X	X	+0.48	+1.79	+1.17
12	X	X	X	X	5%	X	X	X	X	X	X	X	X	-2.75	-1.51	-1.80
13	X	X	X	X	10%	X	X	X	X	X	X	X	X	-3.19	-1.83	-1.97
14	X	X	X	X	15%	X	X	X	X	X	X	X	X	-4.72	-3.83	-4.01
15	X	X	X	X	X	0.05m	X	X	X	X	X	X	X	+1.79	+0.71	+1.14
16	X	X	X	X	X	0.25m	X	X	X	X	X	X	X	+0.76	+0.52	-0.24
17	X	X	X	X	X	0.50m	X	X	X	X	X	X	X	-0.50	-0.08	-1.35
18	X	X	X	X	X	1.00m	X	X	X	X	X	X	X	-0.77	-0.33	-2.02
19	X	X	X	X	X	X	$\pi/20$	X	X	X	X	X	X	+6.08	+4.66	+4.09
20	X	X	X	X	X	X	$\pi/10$	X	X	X	X	X	X	+4.77	+3.63	+2.73
21	X	X	X	X	X	X	$\pi/4$	X	X	X	X	X	X	+7.87	+4.57	+3.06
22	X	X	X	X	X	X	X	[0.95, 1.05]	X	X	X	X	X	+4.98	+3.99	+3.18
23	X	X	X	X	X	X	X	[0.90, 1.10]	X	X	X	X	X	+4.82	+2.83	+1.67
24	X	X	X	X	X	X	X	[0.75, 1.25]	X	X	X	X	X	+4.79	+1.09	-1.49
25	X	X	X	X	X	X	X	X	✓	X	X	X	X	-0.16	+0.67	+0.54
26	X	X	X	X	X	X	X	X	✓	✓	X	X	X	+1.19	+0.09	+1.16
27	X	X	X	X	X	X	X	X	✓	✓	✓	X	X	+1.79	+0.14	-0.45
28	X	X	X	X	X	X	X	X	X	X	X	1	X	+0.96	+1.01	+0.67
29	X	X	X	X	X	X	X	X	X	X	X	5	X	-0.10	+0.29	+0.84
30	X	X	X	X	X	X	X	X	X	X	X	10	X	+0.76	+0.52	-0.48
31	X	X	X	X	X	X	X	X	X	X	X	X	5	+2.71	+2.86	+2.83
32	X	X	X	X	X	X	X	X	X	X	X	X	10	+1.29	+2.59	+1.70
33	X	X	X	X	X	X	X	X	X	X	X	X	15	-0.19	+1.29	+0.64
34	X	X	X	X	X	X	X	X	X	X	X	X	20	+1.72	+1.31	+0.48
35	X	X	X	X	X	X	X	X	X	X	X	X	25	+0.51	+1.01	+0.32
36	0.2m	$\pi/4$	[0.95, 1.05]	✓	X	0.25m	$\pi/20$	X	✓	X	X	5	15	+15.75	+17.72	+16.59
37	0.2m	$\pi/4$	[0.95, 1.05]	✓	X	0.25m	$\pi/20$	X	✓	X	X	5	X	+11.45	+11.06	+10.60
38	X	$\pi/2$	X	X	X	X	X	X	X	X	X	X	15	+13.14	+14.88	+13.88
39	0.2m	$\pi/4$	[0.95, 1.05]	✓	X	X	$\pi/20$	X	✓	X	X	5	15	+15.95	+18.05	+18.30
40	0.2m	$\pi/4$	[0.95, 1.05]	✓	X	X	$\pi/20$	[0.95, 1.05]	✓	X	X	5	15	+16.08	+18.53	+18.51
41	0.2m	$\pi/4$	[0.95, 1.05]	✓	X	X	$\pi/20$	[0.95, 1.05]	✓	✓	X	5	15	+16.95	+19.20	+18.54
42	0.2m	$\pi/2$	[0.95, 1.05]	✓	X	X	$\pi/20$	[0.95, 1.05]	✓	✓	X	5	15	+16.52	+18.83	+17.77

TABLE I

RESULTS OF OUR EXTENSIVE AUGMENTATION STUDY ON THE KITTI [2] VALIDATION SET. MOST SIGNIFICANT IMPROVEMENTS IN **BOLD**.AUGMENTATION POLICY OF POINTPILLARS [1] IN **MAGENTA (#36)**. OUR IMPROVED AUGMENTATION POLICIES IN **CYAN (#39-42)**.

What we report is the new evaluation metric 3D ap₄₀ proposed by Mapillary [23], it is the average precision computed over 40 instead of only 11 recall operation points originally proposed in 2010 by the Pascal VOC benchmark [24]. This new evaluation ensures a more fair comparison. For more details, please refer to their paper [23]. Conformable results of BEV ap₄₀ and 2D ap₄₀ will be published on our website. In this paper we focus on the *car* class and carry out our experiments on the KITTI [2] validation set, following the common practice proposed in [25] to split the official training set into 3,712 training and 3,769 validation samples.

In order to investigate all the potential augmentation techniques introduced in Section III, we have to establish a proper baseline where no augmentation technique is applied (policy #0). To reduce the impact of randomness and to have a more meaningful comparison, we carried out all experiments listed in Table I exactly three times and report the numbers of the training run which has the highest ap₄₀ score on the *moderate* difficulty, the same metric that is used for ranking submissions on the official KITTI leader-board*.

The first finding is, that there is a huge gap (17.72%) between the baseline with no augmentation (policy #0) compared to the augmentation policy used in PointPillars [1] (policy #36). This means that almost $\frac{1}{4}$ (23%) of the performance of PointPillars [1] can be attributed to the sophisticated augmentation policy.

If we look at individual augmentation techniques, most notably we see that *Global Rotation* (policy #4-6) is the most effective augmentation with an increase of up and above 10% (policy #6). Followed by three other *global* augmentation techniques, *Global Translation* (policy #1-3), *Global Scaling* (policy #7-9) and *Random Flip* (policy #10), all contributing with a performance boost of around 7%.

To show how effective *Global Rotation* is as an augmentation technique, we can compare our best performing *Global Rotation* policy (policy #6), with the advanced augmentation policy of PointPillars [1] where only *Oversampling* is removed (resulting in policy #37), and we can see that the two policies perform similarly.

Only adding *Oversampling* to policy #6 (resulting in policy #38) we can already half the gap to the performance of the sophisticated policy (two vs. nine augmentation techniques) utilized in PointPillars [1] (policy #36). On the other hand, *Oversampling* applied by itself (policy #31-35) does not help as much as other individual augmentation techniques. It only shines together with other augmentation techniques, showcasing that the combination of the different augmentation techniques investigated in this paper are not simply additive.

Investigating the remaining *global* augmentation technique *Ground Removal* (policy #11-14), which is intuitive and often performed in classical LiDAR pipelines [26], in our experiments we can see that the augmentation is rather disadvantageous than beneficial.

We speculate that this could be due to two things. First,

it could be due to a lot of context is taken away (especially from the neighborhood of objects) by removing the lowest points of the scene (in such a naive way). Second, it could also mean that “background” points in fact encode more valuable information than what is the established view on that matter. In order to clarify this though, further experiments would be necessary (see discussion in Section V).

In general we see that *local* augmentation techniques are not as effective as *global* augmentation techniques. Although, while *Local Rotation* (policy #19-21) and *Local Scaling* (policy #22-24) can be considered beneficial, *Local Translation* (policy #15-18) contrarily is clearly not as beneficial as the other two *local* augmentation techniques and can even hurt performance if applied too aggressively.

Filter Augmentations (policy #25-30) also do not make a big difference, interesting is maybe only the results of policy #26, where we filter all *hard* examples during training and still get a higher performance on them during evaluation (+1.16%). This could mean that if we keep *hard* examples during training, the network might get too distracted by those seemingly diverse *hard* examples and is not able to extract distinct features from them, thereby hurting its generalisation capabilities.

If we now take all those insights from policy #1-35 and apply them to the augmentation policy of PointPillars [1] (policy #35) we can further boost its performance. First, by removing the potentially hurtful *Local Translation* (resulting in policy #39), then adding *Local Scaling* (resulting in policy #40) and finally also leaving out *hard* examples during training (resulting in policy #41), we can further improve PointPillars [1] by up to 1.5% and in the case of *hard* examples even 2%.

Lastly, policy #42, where we combine all the individual best augmentation techniques from our findings in policy #1-35, shows us (again) that the combination of techniques is not simply additive, as it did not result in the best overall performing technique.

V. DISCUSSION

In this section, we reflect on our findings and discuss the most important ones.

Our extensive study of different data augmentation strategies shows, that there are a few effective single action policies, such as *Global Rotation*, however, the best results can be found by combining the findings of our study to one combined policy. We believe that these findings carry over to other LiDAR datasets that are mentioned in the introduction. Even though most of these datasets are captured with different LiDARs and thereby can have drastically different number of overall LiDAR points per scene (Lyft Level 5 AV Dataset [4] with up to 190,000 points per scene vs. nuScenes [3] that only has on average around 35,000 points per scene). The main issue, the imbalance between “foreground” and “background” points, stays the same for all current LiDAR datasets. The conjecture, that our findings carry over to other LiDAR datasets, is further

*http://www.cvlibs.net/datasets/kitti/eval_object.php?obj_benchmark=3d

backed by the fact that PointPillars [1] trained and evaluated on nuScenes [3] also performs well.

Furthermore, we believe that these augmentation policies do not only hold for PointPillars [1], which is one of the best performing open-source[†] voxel based methods, but does also generalize to other voxel based methods. However, it remains future work to investigate if those findings also hold true for other methods, such as point based methods (see II-B) or point & voxel based methods (see II-C).

Finally, we noted several unexpected outcomes of our augmentations, mainly *Ground Removal* and *Local Translation*, can lower the performance. One possible interpretation is that there is significant information available in the difference between ground and objects. Removing the ground or moving objects too far can destroy this information. Future research is needed to investigate this hypothesis, e.g., by using more sophisticated ground removal techniques or the ground truth of the recently released SemanticKITTI [27] dataset. However, if this hypothesis is true, it could be used to develop new methods that exploit this information.

VI. CONCLUSION & FUTURE WORK

In this work we provide a lot of insight into the effectiveness of different augmentation techniques for LiDAR based 3D Object Detection. We hope that other researches can now take those findings and apply them to their work without going through such a thorough and tedious augmentation study themselves. Further, we uncovered how important data augmentation for LiDAR based 3D Object Detection really is and that it seemingly plays a significant role for all methods we know that are based on the SECOND [13] code-base.

In future work we want to investigate, how transferable such augmentation policies are to other datasets and if transfer learning is possible for LiDAR based 3D Object Detection methods.

REFERENCES

- [1] A. H. Lang, S. Vora, H. Caesar, L. Zhou, J. Yang, and O. Beijbom, "Pointpillars: Fast encoders for object detection from point clouds," in *Proceedings of the IEEE Conference on Computer Vision and Pattern Recognition*, 2019, pp. 12 697–12 705.
- [2] A. Geiger, P. Lenz, and R. Urtasun, "Are we ready for Autonomous Driving? The KITTI Vision Benchmark Suite," in *Proc. of the IEEE Conf. on Computer Vision and Pattern Recognition (CVPR)*, 2012, pp. 3354–3361.
- [3] H. Caesar, V. Bankiti, A. H. Lang, S. Vora, V. E. Liong, Q. Xu, A. Krishnan, Y. Pan, G. Baldan, and O. Beijbom, "nuscenes: A multimodal dataset for autonomous driving," *arXiv preprint arXiv:1903.11027*, 2019.
- [4] J. H. T. P. K. N. A. F. M. Y. B. L. A. J. P. O. S. S. A. K. A. K. C. T. L. P.-s. W. J. R. Kesten, M. Usman and V. Shet, "Lyft Level 5 AV Dataset," <https://level5.lyft.com/dataset/>, 2019.
- [5] P. Sun, H. Kretschmar, X. Dotiwalla, A. Chouard, V. Patnaik, P. Tsui, J. Guo, Y. Zhou, Y. Chai, B. Caine, V. Vasudevan, W. Han, J. Ngiam, H. Zhao, A. Timofeev, S. Ettinger, M. Krivokon, A. Gao, A. Joshi, Y. Zhang, J. Shlens, Z. Chen, and D. Anguelov, "Scalability in perception for autonomous driving: Waymo open dataset," 2019.
- [6] M. Chang, J. Lambert, P. Sangkloy, J. Singh, S. Bak, A. Hartnett, D. Wang, P. Carr, S. Lucey, D. Ramanan, and J. Hays, "Argoverse: 3d tracking and forecasting with rich maps," in *2019 IEEE/CVF Conference on Computer Vision and Pattern Recognition (CVPR)*, June 2019, pp. 8740–8749.
- [7] X. Huang, X. Cheng, Q. Geng, B. Cao, D. Zhou, P. Wang, Y. Lin, and R. Yang, "The apolloscape dataset for autonomous driving," in *Proceedings of the IEEE Conference on Computer Vision and Pattern Recognition Workshops*, 2018, pp. 954–960.
- [8] A. Patil, S. Malla, H. Gang, and Y.-T. Chen, "The h3d dataset for full-surround 3d multi-object detection and tracking in crowded urban scenes," in *International Conference on Robotics and Automation*, 2019.
- [9] "Lidar is getting cheaper," <https://cmte.ieee.org/futuredirections/2019/07/16/lidar-is-getting-cheaper/>, accessed: 2020-03-02.
- [10] Y. Wang, W. Chao, D. Garg, B. Hariharan, M. Campbell, and K. Q. Weinberger, "Pseudo-lidar from visual depth estimation: Bridging the gap in 3d object detection for autonomous driving," *CoRR*, vol. abs/1812.07179, 2018. [Online]. Available: <http://arxiv.org/abs/1812.07179>
- [11] B. Yang, W. Luo, and R. Urtasun, "Pixor: Real-time 3d object detection from point clouds," in *Proceedings of the IEEE conference on Computer Vision and Pattern Recognition*, 2018, pp. 7652–7660.
- [12] Y. Zhou and O. Tuzel, "Voxelnet: End-to-end learning for point cloud based 3d object detection," in *Proceedings of the IEEE Conference on Computer Vision and Pattern Recognition*, 2018, pp. 4490–4499.
- [13] Y. M. Y. Yan and B. Li, "Second: Sparsely embedded convolutional detection," *Sensors*, vol. 18, no. 10, p. 3337, 2018.
- [14] X. Chen, H. Ma, J. Wan, B. Li, and T. Xia, "Multi-view 3d object detection network for autonomous driving," in *Proceedings of the IEEE Conference on Computer Vision and Pattern Recognition*, 2017, pp. 1907–1915.
- [15] J. Ku, M. Mozifian, J. Lee, A. Harakeh, and S. L. Waslander, "Joint 3d proposal generation and object detection from view aggregation," in *2018 IEEE/RSJ International Conference on Intelligent Robots and Systems (IROS)*. IEEE, 2018, pp. 1–8.
- [16] C. R. Qi, H. Su, K. Mo, and L. J. Guibas, "Pointnet: Deep learning on point sets for 3d classification and segmentation," in *Proceedings of the IEEE conference on computer vision and pattern recognition*, 2017, pp. 652–660.
- [17] C. R. Qi, O. Litany, K. He, and L. J. Guibas, "Deep hough voting for 3d object detection in point clouds," in *Proceedings of the IEEE International Conference on Computer Vision*, 2019, pp. 9277–9286.
- [18] A. Dai, A. X. Chang, M. Savva, M. Halber, T. Funkhouser, and M. Nießner, "ScanNet: Richly-annotated 3d reconstructions of indoor scenes," in *Proceedings of the IEEE Conference on Computer Vision and Pattern Recognition*, 2017, pp. 5828–5839.
- [19] S. Song, S. P. Lichtenberg, and J. Xiao, "Sun rgb-d: A rgb-d scene understanding benchmark suite," in *2015 IEEE Conference on Computer Vision and Pattern Recognition (CVPR)*, June 2015, pp. 567–576.
- [20] S. Shi, X. Wang, and H. Li, "Pointcnn: 3d object proposal generation and detection from point cloud," in *Proceedings of the IEEE Conference on Computer Vision and Pattern Recognition*, 2019, pp. 770–779.
- [21] Y. Chen, S. Liu, X. Shen, and J. Jia, "Fast point r-cnn," in *Proceedings of the IEEE International Conference on Computer Vision*, 2019, pp. 9775–9784.
- [22] Z. Liu, H. Tang, Y. Lin, and S. Han, "Point-voxel cnn for efficient 3d deep learning," in *Advances in Neural Information Processing Systems*, 2019, pp. 963–973.
- [23] A. Simonelli, S. R. Buló, L. Porzi, M. Lopez-Antequera, and P. Kotschieder, "Disentangling monocular 3d object detection," in *The IEEE International Conference on Computer Vision (ICCV)*, October 2019.
- [24] M. Everingham, L. Van Gool, C. K. Williams, J. Winn, and A. Zisserman, "The pascal visual object classes (voc) challenge," *International journal of computer vision*, vol. 88, no. 2, pp. 303–338, 2010.
- [25] X. Chen, K. Kundu, Y. Zhu, A. G. Berneshawi, H. Ma, S. Fidler, and R. Urtasun, "3d object proposals for accurate object class detection," in *Advances in Neural Information Processing Systems*, 2015, pp. 424–432.
- [26] J. Kabzan, M. d. I. I. Valls, V. Reijgwart, H. F. C. Hendriks, C. Ehmke, M. Prajapat, A. Bühler, N. Gosala, M. Gupta, R. Sivanesan et al., "Amz driverless: The full autonomous racing system," *arXiv preprint arXiv:1905.05150*, 2019.
- [27] J. Behley, M. Garbade, A. Milioto, J. Quenzel, S. Behnke, C. Stachniss, and J. Gall, "SemanticKITTI: A Dataset for Semantic Scene Understanding of LiDAR Sequences," in *Proc. of the IEEE/CVF International Conf. on Computer Vision (ICCV)*, 2019.

[†]<https://github.com/nutonomy/second.pytorch>